Research Article

Nanocrystals of Novel Valerolactam-Fenbendazole Hybrid with Improved *in vitro* Dissolution Performance

Maria Elisa Melian,[1] Alejandro Paredes,[2] Beatriz Munguía,[1] Maximiliano Colobbio,[3] Juan Carlos Ramos,[3] Ramiro Teixeira,[1] Eduardo Manta,[3,4] Santiago Palma,[2] Ricardo Faccio,[5] and Laura Domínguez[1,6]

Abstract. Valero-fenbendazole (VAL-FBZ) is a novel hybrid compound with *in vitro* anthelmintic activity, designed and synthesized to address the global problem of resistance to anthelmintic compounds. This new molecule derives from fenbendazole (FBZ), a well-known commercially available benzimidazole used in veterinary medicine despite its poor water solubility. In this work, we report for the first time a strategy to solve the solubility problems of FBZ and VAL-FBZ by means of self-dispersible nanocrystals (SDNC). Nanocrystals were prepared by media milling followed by a spray-drying step, and a comprehensive and exhaustive structural and physicochemical characterization was carried out, in order to understand the systems and their behavior. The formulation poloxamer 188 (P188):FBZ 1:1 turned out with the best process yield (53%) and re-dispersability properties, particle size average of 258 nm, and polydispersity index of 0.2 after redispersion in water. The dissolution profile showed a markedly increased dissolution rate compared with the simple mixture of the components (80% FBZ dissolved in 15 min from the SDNC *vs* 14% from the control formulation). FTIR spectroscopy, thermal analysis, and X-Ray Powder Diffraction (XRPD) studies showed no chemical interactions between components and an extensive confocal Raman microscopy analysis of the formulations showed very homogeneous spatial distribution of components in the SDNC samples. This manufacturing process was then successfully transferred for preparing and characterizing VAL-FBZ:P188 (1:1) SDNC with similar results, suggesting the promising interest of a novel anthelmintic with improved biopharmaceutical behavior. In conclusion, new FBZ and VAL-FBZ SDNC with improved dissolution rate were successfully prepared and characterized.

[1] Área de Farmacología, CIENFAR, Facultad de Química, Universidad de la República (Udelar), General Flores 2124, 11800, Montevideo, Uruguay.

[2] Unidad de Investigación y Desarrollo en Tecnología Farmacéutica (UNITEFA), CONICET and Departamento de Ciencias Farmacéuticas, Facultad de Ciencias Químicas, Universidad Nacional de Córdoba, Córdoba, Argentina.

[3] Laboratorio de Química Fina, Instituto Polo Tecnológico de Pando, Facultad de Química, Universidad de la República, By Pass de Rutas 8 y 101 s/n, CP 91000, Canelones, Pando, Uruguay.

[4] Laboratorio de Química Farmacéutica, DQO, Facultad de Química, Universidad de la República (Udelar), Av. General Flores, 2124, Montevideo, Uruguay.

[5] Área Física & Centro NanoMat, DETEMA, Facultad de Química, Universidad de la República (Udelar), Av. General Flores, 2124, Montevideo, Uruguay.

[6] To whom correspondence should be addressed. (e–mail: ldoming@fq.edu.uy)

INTRODUCTION

The intensive use of anthelmintic products has led to global resistance to all commercially available drugs with severe consequences for livestock producing countries (1–5). This widespread resistance also includes Uruguay, where recent reports show an alarming tendency towards the expansion of anthelmintic resistance (6–8). As part of a project to search for new anthelmintic drugs, we have communicated a series of novel valerolactam-benzimidazole hybrid compounds, with interesting *in vitro* activity, but similarly to their benzimidazole precursors, they present extremely low water solubility (9,10).

Poor water solubility remains an important challenge for the development of new drugs, since it can lead to poor or erratic oral absorption and consequently to suboptimal therapeutic performance (11). Different processes have been designed to increase solubility, dissolution rate, and bioavailability of hydrophobic active pharmaceutical ingredients (APIs), with focus on those classified as classes II and IV in the biopharmaceutical classification system (BCS). Some classical formulation strategies that have been explored include liposomes (12), micelles (13), co-crystals (14), and cyclodextrins (15), among others.

More recently, novel nanoformulations such as nanoparticles (16), solid dispersions (17), nanoemulsions (18), and nanogels (19) have been also reported. Among all available strategies, nanocrystals (NCs) have made a major academic and industrial impact, since first reported (20–22). NCs are nanoparticles composed of 100% drug, usually surrounded by a stabilizer layer which acts as soluble link among the drug particles, enabling its redispersion after contact with an aqueous solvent (i.e., gastrointestinal fluids) (23–26). NCs' key features are based on their reduced particle size, which produces a sharp increase in the specific surface area, giving them mucoadhesive properties, while decreasing the diffusion layer thickness leading to an increase in the extent and rate of drug dissolution (24,27). Nanoparticles in solution are quite unstable because of the extra Gibbs free energy contribution related to reducing particle size and increasing surface energy (28). They tend to agglomerate to minimize their total energy when formulated as liquids, but this problem can be solved by the addition of a correct type and amount of stabilizer (29).

Nanocrystal production technologies can be classified as top-down or bottom-up. Bottom-up processes imply the growth of drug clusters from an atomic level (i.e., drug dissolution in a suitable medium, followed by precipitation or drying). Top-down approaches refer to the reduction of the particle size of the bulk drug in order to get nanosized particles using a mechanical method (i.e., media milling or high-pressure homogenization) (17). Moreover, the combination of bottom-up and top-down technologies has also been developed (30). Among the top-down techniques, the wet bead milling is one of the most frequently used for drug nanocrystals production (31) and is currently reported as a high efficiency and low cost technique (32–34). The drug, stabilizer, milling media, and solvent are stirred under controlled temperature, allowing to obtain drug suspensions highly uniform in particle sizes and within the sub-micrometer range. It is interesting to note that as a part of the process of wet bead milling, the obtained nanosuspension, properly stabilized, could be used as a liquid formulation in the form of injectables, oral suspensions, etc. (35). Otherwise, the obtained nanosuspension can be dried and converted into redispersible powders, being the spray-drying technique one of the most cost-effective processes commonly used to this purpose (25,36,37).

Recently, we have reported the manufacturing and characterization of solid dispersions of a poorly water-soluble drug, fenbendazole (FBZ), in order to improve its dissolution rate, with promising results (8). This drug belongs to the broad-spectrum benzimidazole (BZ) anthelmintic class, worldwide used for the treatment of parasitic diseases in human and veterinary medicine, despite their low bioavailability (38–40).

In this work, we report for the first time a strategy to overcome the solubility problems of FBZ and valero-fenbendazole (VAL-FBZ, one of the new compounds patented by the group, Fig. 1, (41)). FBZ and VAL-FBZ NCs were prepared by wet bead milling followed by a spray-drying step, and a comprehensive physicochemical characterization was carried out, including confocal Raman microscopy, thermal analysis, X-ray powder diffraction FTIR spectroscopy, and dissolution assays.

MATERIALS AND METHODS

Materials

Fenbendazole (FBZ, pharmaceutical grade) and its marketed suspension (MS) were kindly provided by Laboratorio Uruguay S.A. (LUSA, Montevideo, Uruguay). Poloxamer 188 (P188) and poloxamer 407 (P407) were provided by BASF (Ludwigshafen, Germany). For the milling process, Zirmil® Yttria-stabilized zirconia beads of two different sizes (0.15–0.28 and 0.4–0.6 mm) (Saint-Gobain ZirPro Kölh, Germany) were used. Mannitol, lactose,
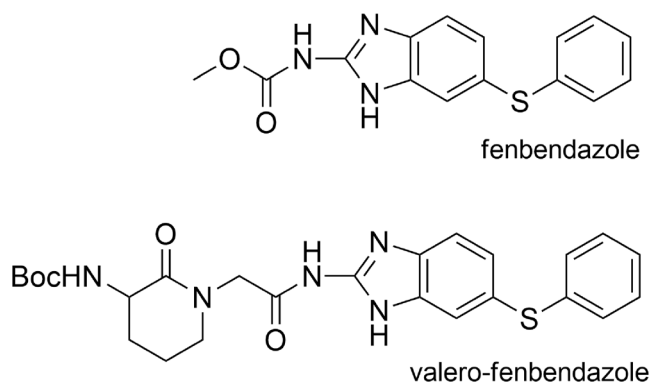

Fig. 1. Fenbendazole and valero-fenbendazole structures

hydroxypropyl methylcellulose (HPMC, METHOCEL™ E5 Premium LV), and polyvinylpyrrolidone (PVP-k30) were of pharmaceutical grade. Valero-fenbendazole (VAL-FBZ) was produced by the collaboration between the groups of Medicinal Chemistry and Pharmacology from Facultad de Química, Universidad de la República, Uruguay (DNPI, n° 14,424) (9); a brief scheme of the chemical synthesis is described in supplementary data. All other reagents were of analytical grade.

Methods

Preparation of FBZ and VAL-FBZ Nanosuspensions (NSs)

Drug nanosuspensions (NSs) were prepared by wet bead milling using a NanoDisp® laboratory-scale mill (NanoDisp, Córdoba, Argentina). The device consisted of a sealed jacketed grinding chamber and a shaft coupled to a motor. First, mixtures of drug and different carriers (HPMC, PVP, Lactose, Mannitol, P407 or P188) in 1:1 ratio (Table 1) were grounded in a mortar and ultrapure water was gradually added up to 200 mL to form a homogeneous suspension. Also, for P188 different NSs were prepared by decreasing the amount of stabilizer (33, 20, and 10%). Afterwards, drug suspensions and zirconia beads (particle size 0.5 mm or 0.1 mm) were placed in the milling chamber and processed at approximately 1600 rpm for 2 h, according to the previous experiences reported (42,43). Samples were taken every 30 min for particle size and polydispersity index (PDI) evaluation.

Preparation of Self-Dispersible Nanocrystals (SDNCs)

The spray-drying process was performed on a laboratory-scale Mini Spray-dryer Büchi B-290 (Büchi Labortechnik AG, Switzerland) equipped with a dehumidifier module, following an experimental set-up reported previously (25). A two-fluid nozzle with a cap orifice diameter of 1.5 mm was used, and the operating conditions were atomization air (L/h), 50; aspiration (m^3/h), 75%; temperature (°C), 45; and pump (mL/min), 5.

Preparation of Drug Physical Mixtures (PMs)

Control physical mixtures of drug and carrier were prepared in order to compare the SDNCs against the simple mixture of its components. PMs were prepared by manually mixing the appropriate amount of FBZ or VAL-FBZ and carrier previously pulverized and sieved to a maximum particle size of 250 μm.

Characterization

Process Yield Determination. Full process (FP) yield was determined by weighting the powder obtained after the drying step and comparing it with the weight of the starting material (100%). These FP yield estimations help assess the global mass loss produced during the different manufacturing steps (e.g., product separation from the milling bed, transfers among containers, and drying). Specifically, the drying step yield was calculated weighting the suspensions before drying

to consider the amount of solid in it as 100% and comparing it with the weight of dry powder obtained after the spray-drying process.

Particle Size and Polydispersity Index (PI) Measurements

The particle size and PI values of FBZ and VAL-FBZ nanocrystal suspensions and their corresponding redispersed SDNCs (approximately 1 mg of SDNCs were resuspended in 5 mL of water) were determined by dynamic light scattering (Zetasizer Nano-Zs®, Malvern Instruments, UK). Before taking measurements, the samples were properly diluted with deionized water in order to standardize nanocrystal concentration.

Moisture Content

The powder moisture content was measured immediately after the spray-drying step in a moisture analyzer with halogen heating (OHAUS M45VR).

Scanning Electron Microscopy

Scanning electron microscopy images of pure components, the SDNCs, and the PMs were taken by scanning electron microscopy (SEM). Samples were attached to adhesive conducting tape and sputtered with Au before examination using a scanning electron microscope (ZEIZZ, Sigma, Germany).

Confocal Raman Microscopy

Confocal Raman microscopy was performed using WITec Alpha 300-RA confocal Raman spectrometer equipment. The excitation laser wavelength corresponds to $\lambda = 532$ nm, and the power was adjusted to 45 mW to avoid sample decomposition. Raman spectra were obtained by averaging a set of 3.600 spectra with 0.133 s integration time for each spectrum. The spectrometer operating with a grating of 600 lines/mm allowed us to obtain spectrums with resolution of ~4 cm^{-1} in the range of 70–4000 cm^{-1}. All the images were collected at the resolution optical limit of ~300 nm.

Principal component analysis (PCA) and peak to peak intensity ratio normalization, adapted from Karavas *et al.* (44), were used for analyzing the spatial distribution of FBZ and VAL-FBZ in the samples.

X-Ray Powder Diffraction (XRPD)

X-ray powder diffraction (XRPD) was performed using Rigaku Ultima IV diffractometer operating in a Bragg-Brentano geometry, with CuKα (λ=1.5418 Å) radiation measuring the $2\theta = 2.00$–$60.00°$ range using 2θ steps of $0.02°$ with a 10 s integration time per step.

Table 1. Composition of the Prepared Fenbendazole and Valero-Fenbendazole Nanosuspensions

Formulation	FBZ (g)	VAL-FBZ (g)	P188 (g)	HPMC (g)	P407 (g)	PVP-k30 (g)	Lactose (g)	Mannitol (g)	Zirconia beads size (mm)
NS1	5.0	–	5.0	–	–	–	–	–	0.5
NS2	5.0	–	2.5	–	–	–	–	–	0.5
NS3	5.0	–	1.2	–	–	–	–	–	0.5
NS4	5.0	–	0.5	–	–	–	–	–	0.5
NS5	5.0	–	–	5.0	–	–	–	–	0.5
NS6	5.0	–	–	–	5.0	–	–	–	0.5
NS7	5.0	–	–	–	–	5.0	–	–	0.5
NS8	5.0	–	2.5	–	–	–	2.5	–	0.5
NS9	5.0	–	2.5	–	–	–	–	2.5	0.5
NS10	2.5	–	2.5	–	–	–	–	–	0.1
NS11	–	2.5	2.5	–	–	–	–	–	0.1

Thermal Analysis

Thermogravimetric (TGA) and differential scanning calorimetry (DSC) curves were obtained using a Jupiter STA 449, Netzch simultaneous thermal analysis equipment. A sample of around 5 mg was placed in sealed aluminum crucibles with pierced lids. Measurements were made from 30°C up to 300°C using a heating rate of 5°C/min. The sensors and the crucibles were under a constant flow of nitrogen (50 mL/min) during the experiment. The fusion and decomposition temperatures were taken as the extrapolated onset temperature of the endothermic/exothermic peak.

Fourier Transform Infrared Spectroscopy

Fourier transform infrared spectroscopy (FTIR) was performed using FTIR spectrometer IR-Prestige 21 (Shimadzu, Japan). The formulations were characterized using KBr disks from 4000 to 500 cm^{-1}, at a resolution of 2 cm^{-1}.

FBZ and VAL-FBZ Dissolution Assay

In vitro drug release studies of pure drugs, SDNCs, and their respective PMs were performed under sink conditions (equivalent to 5 mg of FBZ or 8 mg of VAL-FBZ, according to saturation solubility experiments), in a USP dissolution apparatus 2 (SR6 SR11–6-Flask Dissolution Test Station, Hanson Research), using 900 mL of HCl 0.1 N as dissolution medium, stirred at 50 rpm and at 37.0°C. The filtered sample solutions (0.45 μm) were collected at 3, 5, 10, 15, 30, and 60 min, filtered again through 0.22 μm pore membranes, and analyzed for drug content using a UV-visible spectrophotometer (Genesys 10S UV-Vis Spectrophotometer, Thermo Fisher Scientific) at 289.5 nm and 296 nm for FBZ and VAL-FBZ, respectively, according to our previous communication (8). The dissolution efficiency (DE) of each formulation was estimated at different dissolution times (5, 30 and 60 min) according to the equation described by Khan and Rhodes (45).

FBZ and VAL-FBZ Saturation Solubility Experiments

Excess amounts of pure drug, PMs and SDNCs containing 50% of P188 (equivalent to approximately 5 mg of drug) were dispersed in 5 mL of 0.1 N HCl (6 replicates) and stirred at 37°C for 72 h using a shaker incubator (MRC-LM 570, MRC Ltda). The filtered sample solutions were analyzed using a UV-visible spectrophotometer at 296 nm after appropriate dilution.

RESULTS

Preparation of FBZ and VAL-FBZ Nanosuspensions

Drying and FP yields, moisture content, and drug particle size before and after the spray-drying process are

Table 2. Process Yields, Moisture Content of the SDNCs Prepared, and FBZ and VAL-FBZ Particle Size Before and After the Spray-Drying Process

Formulation	Yield (%)		Moisture content (%)	NS drug particle size before drying		SDNCs particle size (after drying and redispersing)	
	FP	Drying step		D (nm)	PI	D (nm)	PI
SDNC1	53	74	1.08	466.8	0.3	418.5	0.3
SDNC2	34	44	0.33	537.5	0.1	791.0	0.5
SDNC3	18	20	0.59	580.7	0.3	1258.3	0.3
SDNC4	15	21	1.18	540.0	0.2	2033.3	0.3
SDNC5	39	61	2.5	783.8	0.2	693.4	0.2
SDNC6	44	60	0.79	511.5	0.3	307.0	0.2
SDNC7	41	56	5.76	432.7	0.2	757.2	0.5
SDNC8	1	1	**	521.1	0.3	612.3	0.3
SDNC9	33	39	0.89	411.5	0.2	363.9	0.2
SDNC10*	60	73	1.35	265.9	0.2	258.1	0.2
SDNC11*	63	72	2.08	215.4	0.2	217.0	0.2

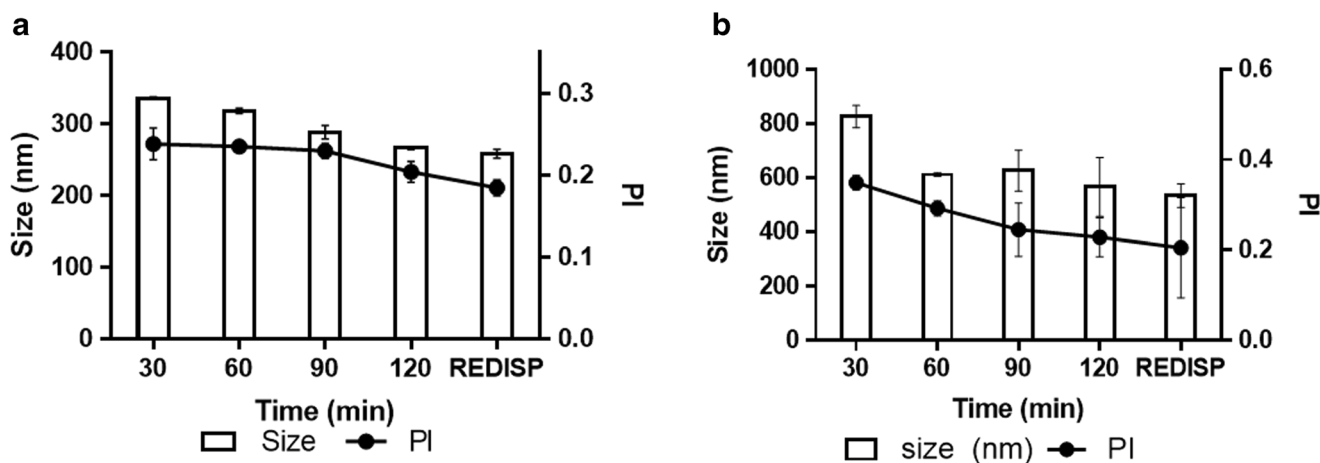*Prepared with a zirconium bed of 0.1 mm size (see experimental section)
**Not measured

Fig. 2. a VAL-FBZ particle size (nm) and PI of the nanosuspension (NS) during the 2-h grinding process and VAL-FBZ particle size after drying and redispersion of the SDNC. **b** Idem for FBZ size and PI in the NS and redispersed SDNC

summarized in Table 2. From the first set of FBZ SDNCs prepared with a bead size of 0.5 mm, the spray-dried formulation containing 50% of P188 showed the best drying yield (74%), followed by those containing HPMC, P407 and PVP-k30 (61, 60, and 56%, respectively).

During the 2-h milling time, particle size and IP of all the different formulations were found to follow a decreasing trend (Fig. 2), and submicron drug particles were obtained with all stabilizers.

According to the mentioned results, P188 was selected among the stabilizers used for further studies. The influence of different amounts of polymer on the nanocrystal production was assessed preparing FBZ nanosuspensions decreasing the amounts of P188 (33, 20, and 10%, NS2, NS3, and NS4, respectively). Variations in the polymer concentration did not impact the FBZ particle size in the NS (after the milling process), but they markedly decreased the yield of the drying step and affected the size of the FBZ redispersed SDNCs (after the drying step, Table 2).

Once selected the carrier and its optimal concentration (P188 at 1:1 ratio), FBZ and VAL-FBZ SDNCs, were prepared using a bead milling of 0.1 mm. Drying and FP yields, moisture content, and drug particle size before and after the spray-drying process are also summarized in Table 2.

Focusing on the final particle size of the FBZ P188 1:1 formulations (SDNC1 and SDNC10), the outcome of varying the size of the zirconium milling bead is clear: smaller drug nanoparticles were obtained with the 0.1-mm zirconium bead (SDNC10) compared with the same composition formulation prepared with a 0.5 mm bead (SDNC1).

Confocal Raman Microscopy

Raman spectra of pure FBZ, VAL-FBZ, and P188 were collected (Fig. 3). The Raman analysis of pure components aided in the identification of differential Raman signals, some specific to the drugs (around 1550 cm^{-1}), and others to the carrier (around 841 cm^{-1}).

The procedure to obtain two-dimensional (2D) confocal Raman microscopy images was performed on both FBZ and VAL-FBZ SDNCs with 50% P188 (SDNC10 and SDNC11) and the corresponding PMs at random locations in areas of

10×10 um, with a grid of 60×60 points defining the bitmap image. Single Raman spectra for every pixel of the selected areas were collected. The obtained Raman mapping of both components of each formulation are shown in Fig. 4. These images show the high homogeneity achieved in the NCs during the nanonization process compared with the corresponding PMs.

The processing of the collected spectral data included the generation of a normalized image in terms of peak intensity ratios to avoid point-to-point variations produced by height differences on the sample surface (8) and a principal component analysis image.

In order to obtain the normalized image of VAL-FBZ SDNCs and PM, the selected signals were 1571 cm^{-1} for VAL-FBZ and 841 cm^{-1} for P188, and the ratio was calculated as I_{1571}/I_{841} (Fig. 5). We proceeded with scripts prepared in our group to obtain the histograms of the different intensity ratio distributions (8). The normalized image for the VAL-FBZ SDNCs showed homogeneous distribution of the VAL-FBZ/P188 ratios, indicating that the composition of the sample was very similar in each pixel of the selected area (down to the diffraction limit of 300 nm). The
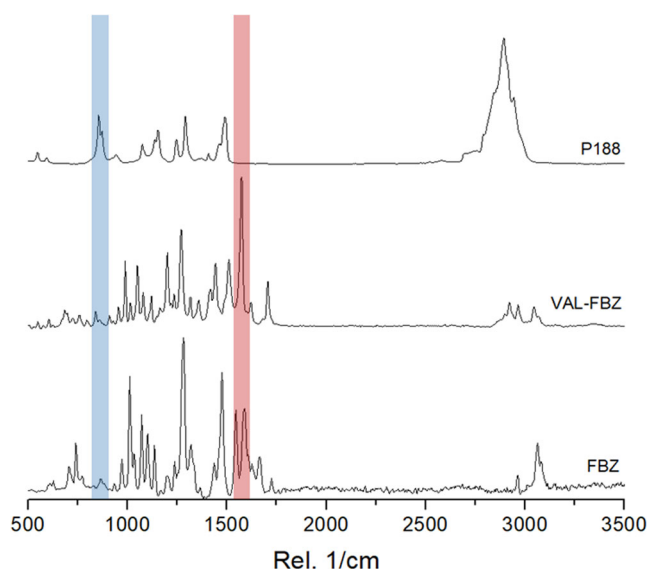

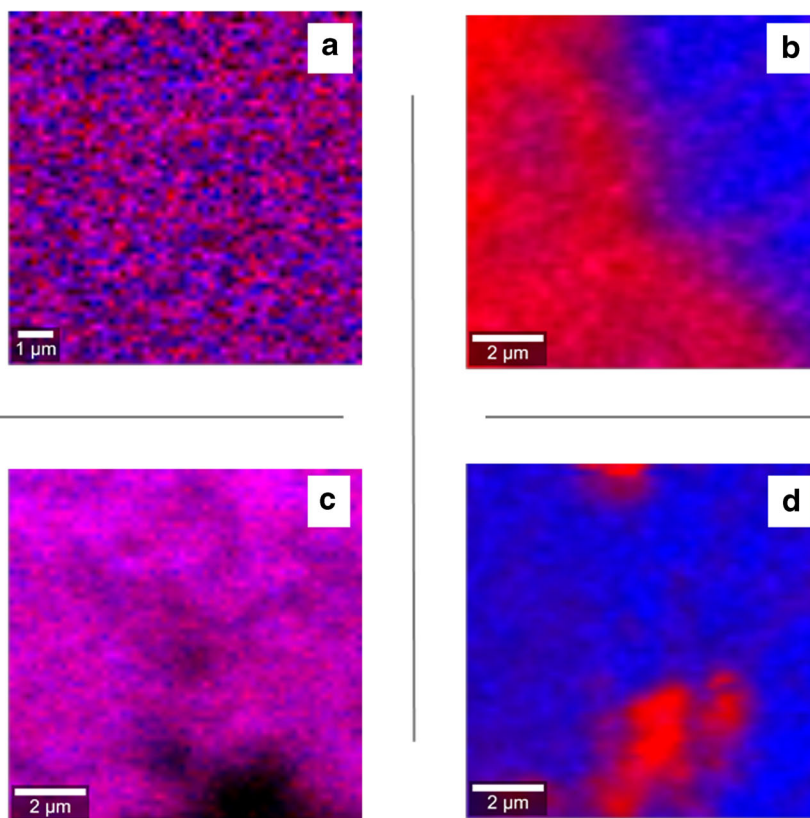**Fig. 3.** Raman spectra for P188, VAL-FBZ, and FBZ

Fig. 4. Reconstructed Confocal Raman mapping images showing de active zone (red) and PMs region (blue) for **a** NC VALFBZ, **b** PM VAL-FBZ, **c** NC FBZ, and **d** PM FBZ

histogram shows a distribution of the density of ratios with normal-like distribution. The VAL-FBZ PM normalized image shows areas where P188 predominates and others richer in VAL-FBZ.

For the FBZ SDNC10 and PM, the selected signals to obtain the normalized image were 1591 cm^{-1} for FBZ and 841 cm-1 for P188, and the ratio was calculated as I1591/I841 (Fig. 6). The FBZ SDNC10 and PM normalized analysis was analogous to that described for VAL-FBZ.

The principal component analysis (PCA) images of the samples were obtained by processing the same spectral data used to calculate the normalized I_{1591}/I_{2878} 2D confocal Raman mapping images. In the analysis of the FBZ PM, PCA imaging allowed us the identification of areas containing mainly FBZ or P188 and a small zone where both components are detected. In the FBZ SDNC10 formulation, even though PCA detects some differences in the image, the mean spectrum calculated is the same for the different areas, indicating that the sample is highly homogeneous.

In the analysis of VAL-FBZ PM, the PCA reconstructed image allowed us the identification of areas containing mainly VAL-FBZ or P188 and a small zone where both components are detected (Fig. 7). The PCA of the VAL-FBZ SDNCs was not able to find statistical differences among the pixels (data not shown).

Scanning Electron Microscopy (SEM)

VAL-FBZ formulations SEM results are shown in Fig. 8. SEM images of VAL-FBZ showed a regular needle-shaped crystalline solid with a distribution size of 2–20 μm and a smooth surface, while the carrier micrographs showed smooth surface spherical particles of 200–500 μm. On the other hand, the VAL-FBZ SDNCs consist of spherical particles with homogeneous diameter in the range of 2–5 μm. FBZ SEM results are shown in supplementary data.

FTIR, XRPD, and Thermal Analysis

DSC and TGA results showed that P188 melts at 50°C and FBZ melts with decomposition at 210°C (Fig. 9); this makes measuring the heat of fusion above 200°C intricated. In fact, there are no differences among the TGA thermograms for the PM and SDNCs' formulations of equal composition, suggesting that there are no relevant interactions between polymer and drug. The thermal characterization of the VAL-FBZ and P188 formulation was analogous to the one described for FBZ. This complementary information is shown in supplementary data.

From the more relevant infrared signals corresponding to pure FBZ (3336.12; 1630.31; 742.28; 685.11 cm-1) and P188 (2881.43; 1281.52; 1117.75 cm-1), those that were exclusive signals of each component remain clearly unaltered in the SDNCs and the respective PM collected spectra, suggesting the absence of chemical interactions between the components in the different formulations (Fig. 10).

This observation was confirmed by XRPD (Fig. 11) where the diffractograms of the FBZ SDNCs and PM showed the signals assigned to each pure component unchanged (FBZ: $2\theta(°) = 6.68$, 11.16, 13.36; P407: 2theta(°) = 19.18, 23.36).
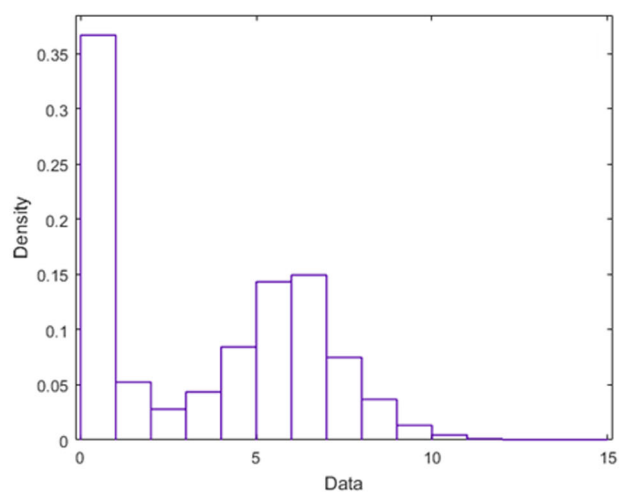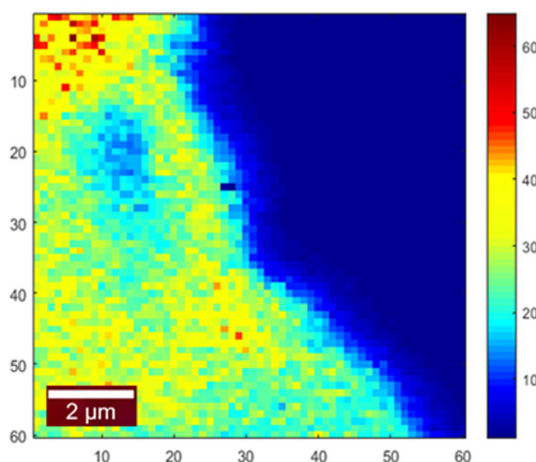
VAL-FBZ SDNC
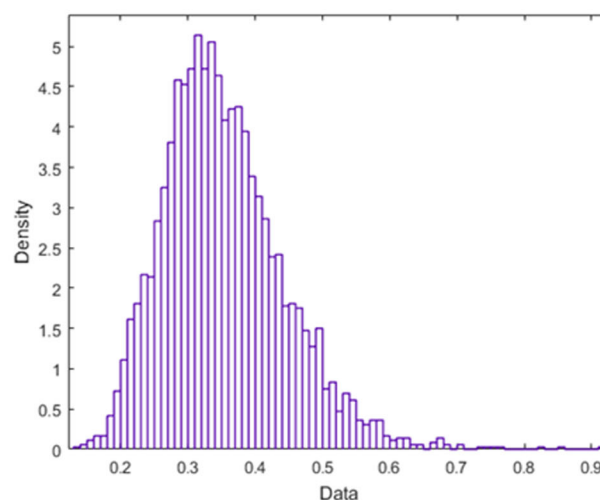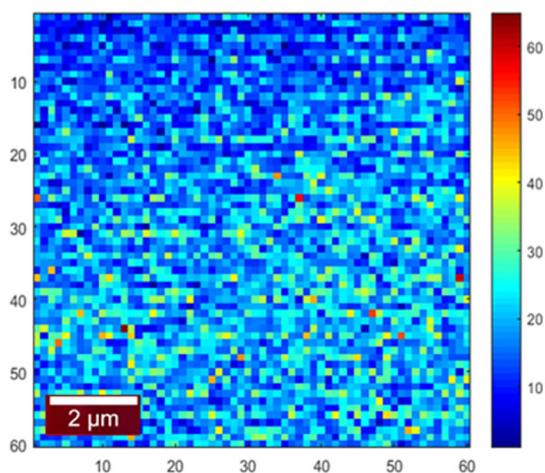
VAL-FBZ PM

Fig. 5. XY confocal Raman microscopy mapping images of VAL-FBZ PM and SDNC; the corresponding histograms of the distribution of VAL-FBZ/P188 ratios are shown on the right. Scale bars indicate the intensity ratio I_{1571}/I_{840}. All images include the number of grid points in X and Y axis and the corresponding bar length

For VAL-FBZ, XRPD studies showed some changes in the relative intensity, and the position of some of the VAL-FBZ peaks in the VAL-FBZ SDNCs diffractogram (pure VAL-FBZ: $2\theta(°) = 4.31$, 8.71, 8.84, 10.79, 12.45, 15.51), suggesting that possible changes occur in the crystal structure (Fig. 12).

Thus, experiments were performed by mixing pure VAL-FBZ and water in a mortar and drying the suspension in a heater. The analysis of this water-processed sample showed the same XRPD pattern of VAL-FBZ SDNCs (pure VAL-

FBZ-water-processed: $2\theta(°) = 4.35$, 4.64, 8.72, 9.30, 11.50, 12.43, 13.56, 15.41, 16.25), suggesting that a new (or modified) crystalline phase structure of VAL-FBZ was obtained after the water treatment in a very reproducible way (Fig. 13).

The signals around 3300 cm^{-1} present in pure VAL-FBZ and the VAL-FBZ P188 1:1 PM shifted to lower wavenumbers after the nanomilling process (VAL-FBZ SDNCs sample, Fig. 14). Moreover, the FTIR spectrum of the water-processed sample showed the same FTIR shift observed for the SDNCs' sample (Fig. 15).
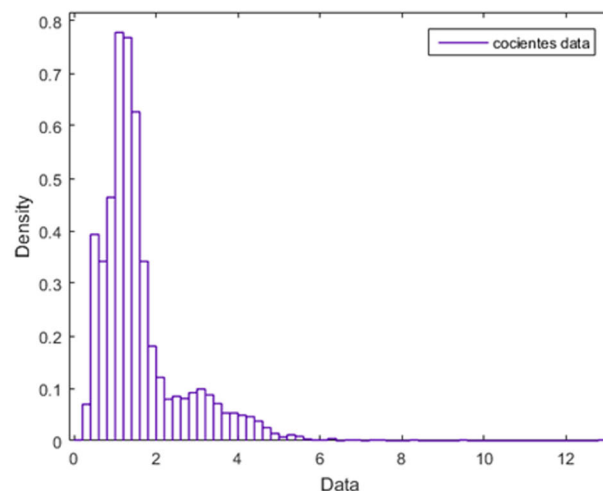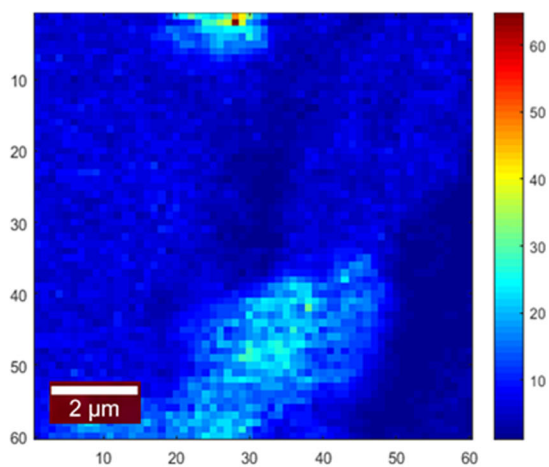
FBZ SDNC
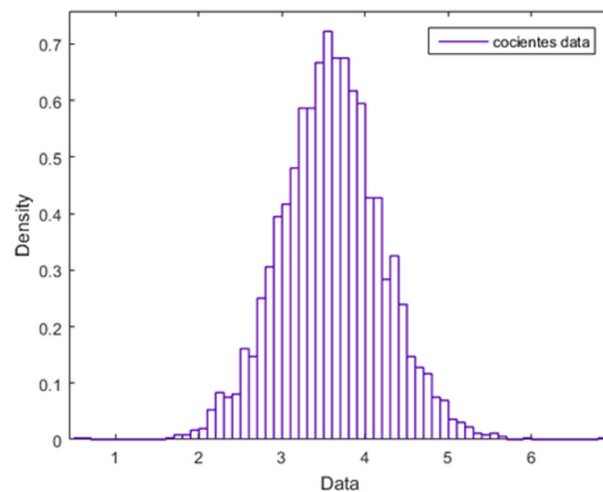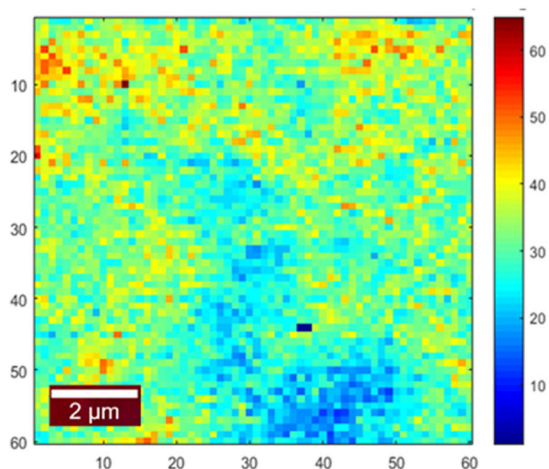
FBZ PM

Fig. 6. XY confocal Raman microscopy mapping images of FBZ PM and SDNC; the corresponding histograms of the distribution of FBZ/P188 ratios are shown on the right. Scale bars indicate the intensity ratio I_{1591}/I_{841}. All images include the number of grid points in X and Y axis and the corresponding bar length

The signals corresponding to P188 do not present any changes neither in the SDNCs' XRPD pattern nor in their FTIR spectrum respect to the pure P188 studies, reinforcing the idea that there is no interaction between polymer and drug, but there is a change in the drug crystalline structure. This fact is also supported by the Raman spectroscopy analysis, where no relevant changes were observed for VAL-FBZ and VAL-FBZ SDNCs' sample.

Saturation Solubility Experiments

The results of the saturation solubility experiments are shown in Table 3. As it was reported previously for albendazole, another compound of the benzimidazole family, the final concentration of P188 achieved during the solubility assay (lower than 0.1% w/v) does not affect the drug solubility in HCl 0.1 N, at the temperature tested (25,26,46). However, the solubility of the SDNCs' preparation was significantly higher than both the pure drugs and the respective PMs.

Dissolution of FBZ and VAL-FBZ Formulations

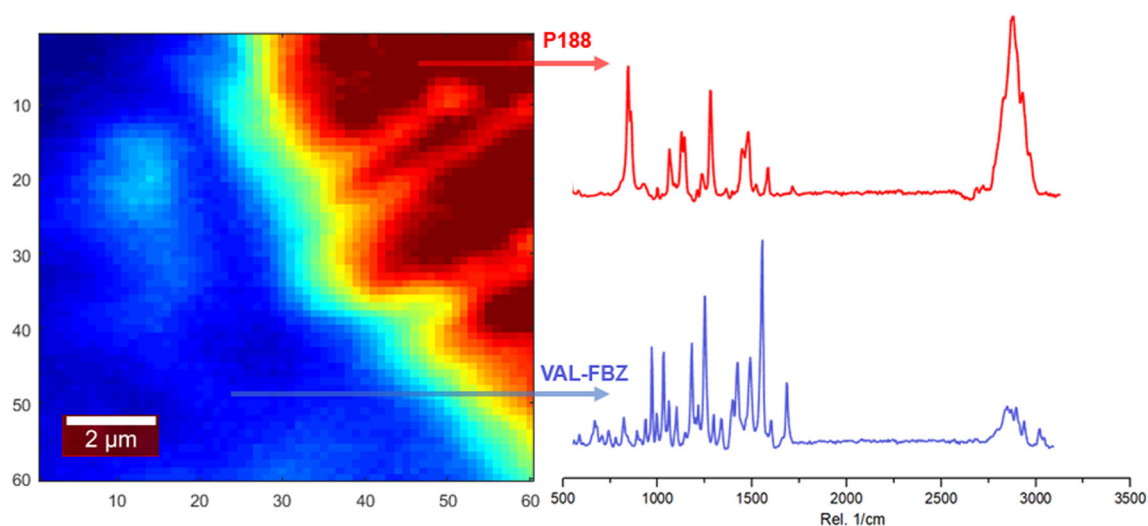The dissolution assays were carried out for pure drugs (not formulated), FBZ and VAL-FBZ SDNCs' formulations,

Fig. 7. Example of PCA-reconstructed image of VAL-FBZ PM considering PC1. The shown spectra were the calculated mean spectrum of the blue colored area and red colored area

the corresponding PMs and a conventional FBZ-marketed suspension (MS).

Dissolution profiles of VAL-FBZ, FBZ and their 1:1 poloxamer formulations are shown in Fig. 16. During the first 15 min of the assay, the amount of pure drug could not be quantified, while FBZ and VAL-FBZ dissolved from SDNCs reached around 85% of the total amount of assayed drug. The amount of drug dissolved from the nanocrystal formulations doubled the amounts dissolved from the PMs during the complete assay. For the marketed suspension, scarcely 40% of the FBZ contained was dissolved in the same period.

The profiles were statistically compared using a model independent approach, calculating the difference factor (F1) and the similarity factor (F2). The calculated factors for the FBZ curves showed that all the formulations presented different dissolution profiles (data not shown).

The dissolution efficiency (DE) of each formulation was estimated at different dissolution times (5, 30 and 60 min) and is summarized in Table 4. As it shows, SDNCs of both drugs presented the highest DE for the different dissolution times selected.
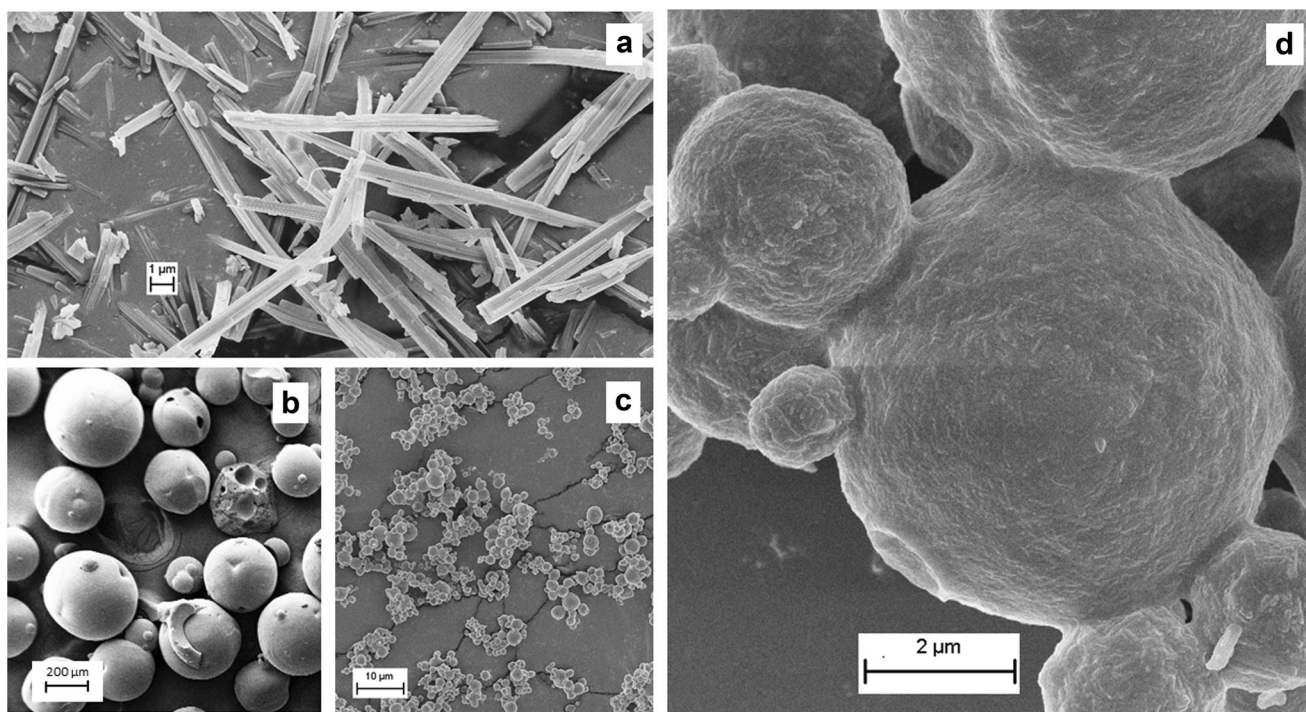

Fig. 8. SEM images for **a** Pure VAL-FBZ 4.00 K X, **b** Pure P188 24 X, **c** SDNC VAL-FBZ 1.00 K X, **d** SDNC VAL-FBZ 8.00 K X
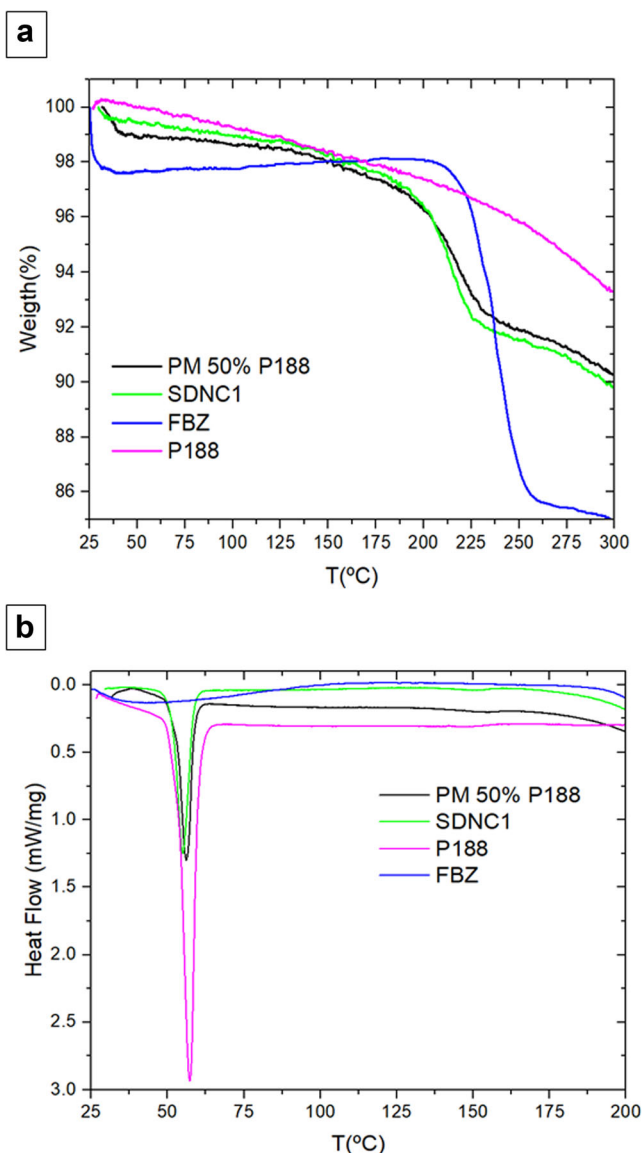
Fig. 9. Thermal analysis. **a** TGA analysis for FBZ:P188 formulations and pure components. **b** DSC analysis for FBZ:P188 formulations and pure components

Fig. 10. FTIR of FBZ:P188 1:1 formulations and pure components

DISCUSSION

Preparation of SDNCs of FBZ and VAL-FBZ

The milling process was successful since all nanosuspensions presented drug particle sizes above the submicron range, independently of the amount or type of stabilizer used. However, from the results of drying yields presented in Table 2, it can be understood that the type of stabilizer plays a major role during the spray-drying step, for the selected drying conditions. In this work, the drying conditions during the spray-drying process were selected based on previous experiences of the group (25),
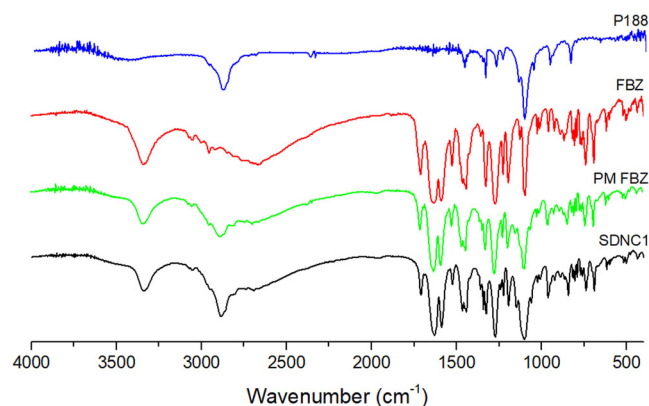
where it was demonstrated that these conditions are crucial for obtaining high process yields. Further studies could be done in order to optimize the spray-drying operating conditions for each particular stabilizer.

Besides the influence of the type of stabilizer in the process yield, the amount of excipient used also plays a major role in the redispersion process. It was noticed how decreasing the amount of P188 from 50 to 10% makes the redispersion process less efficient. This remarks the importance of optimizing the amounts of these kinds of stabilizers which act as soluble covers for the nanocrystals and have a protective effect during the spraying. Higher proportions of stabilizer may prevent irreversible aggregation of drug particles, acting as a stronger soluble links during the drying process, protecting particles from aggregating due to the high kinetic energy and shear forces that take place during the drying step (25,47).

These findings are in line with reports by other authors who have been able to elucidate how stabilizers can impact stability of nanocrystals and improve drying and redispersion performance. The use of P188 as a stabilizer is not trivial since, in addition to promoting the stability of the system, this polymer can increase the dissolution rate of drugs by modifying the hydrodynamic environment (48,49).

The results of transferring the SDNCs' preparation procedure optimized with FBZ to its hybrid drug VAL-FBZ were as expected. VAL-FBZ P188 1:1 SDNCs were obtained with the same process yields and particle size as it was achieved for FBZ, and the redispersion behavior of the VAL-FBZ SDNCs was analogous to those of FBZ.

Physicochemical Characterization

For FBZ, chemical interactions among the components of the formulations were discarded since FTIR and Raman spectroscopic studies, thermal analysis, and XRPD showed no differences between the SDNCs and the corresponding PM samples. In the case of the formulations containing VAL-FBZ, it was found that some changes occur in the XRPD pattern of the SDNCs *vs* the PM, accompanied by a slight
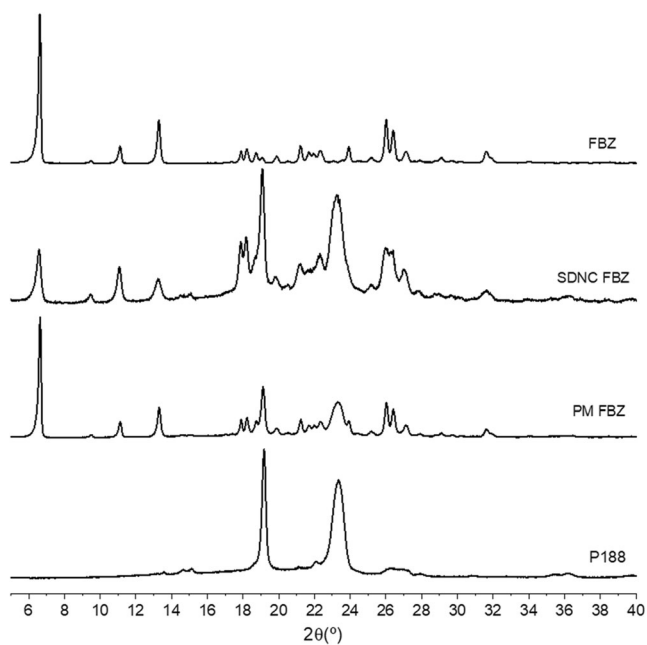
Fig. 11. XRPD. Formulations containing FBZ:P188 in the ratio 1:1 and pure components

shift of one of the FTIR spectroscopic signals. This fact could be attributed to some polymorphic transformation or a possible hydrate formation during the NC formulation process. In order to assess the effect of the NC formation process in the crystalline structure of the original VAL-FBZ, we evaluated the potential incorporation of water molecules to the structure or its possible changes performing mechanical
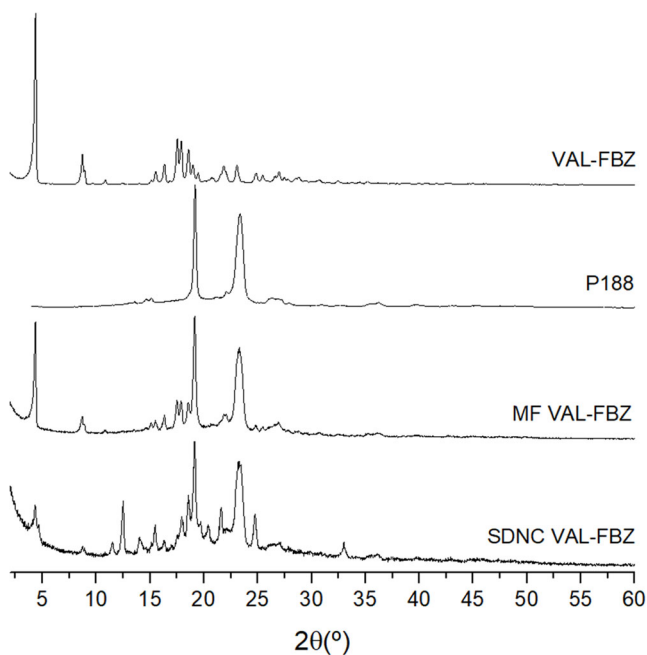
activation in the presence of water by wet bead milling. This hypothesis is totally aligned with the shift observed in the signals assigned to the N-H vibrations in the FTIR spectra. This shift could be explained in terms of hydrogen bond formation in the new crystal lattice. It is well documented that the formation of hydrogen bonds results in changes of the vibrational spectra of the molecules involved where the absorption band of the stretching mode of the X − H donor group (being X an electronegative atom, in this case N) displays the most prominent modifications, a shift to lower wavenumbers, and in most cases a substantial spectral broadening and reshaping (50).

Saturation Solubility and Dissolution Performance

The saturation solubility of the SDNCs' preparation was significantly higher than both the pure drugs and the respective PMs. This phenomena of saturation solubility being a function of particle size was already reported and explained by Keck and Müller (2006) for compounds with particle size below 1 mm (23), based in the Ostwald-Freudlich and Prandtl equation.

Weak bases as benzimidazole drugs, including FBZ, largely depend on their dissolution in the acid environment of the stomach to later assure their absorption in the first part of the duodenum (51,52). In terms of dissolution performance, the SDNCs formulations doubled the amount of drug released and dissolved compared with the respective control PM and a commercially available FBZ conventional suspension. In this sense, SDNCs count with many advantages that contribute to their improved dissolution rate, besides the known positive effect of the enlarged surface area of the drug powder. It was verified the increased saturation solubility of both drugs when formulated as NCs, which has been previously related to an improved dissolution velocity,
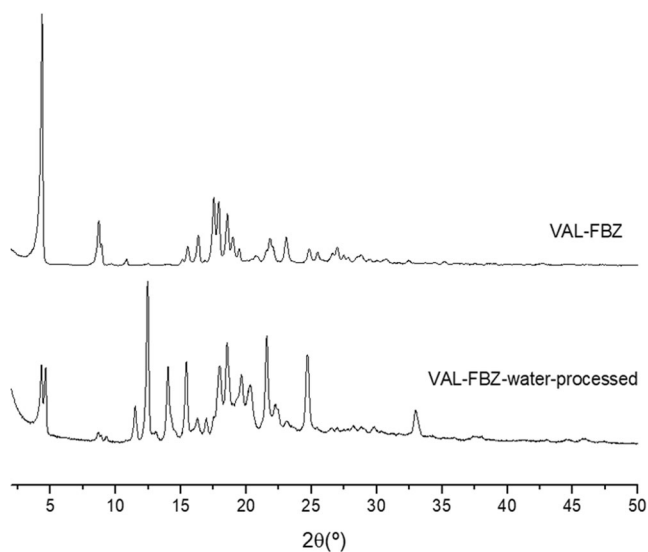

Fig. 12. XRPD. Formulations containing VAL-FBZ:P188 in the ratio 1:1 and pure components

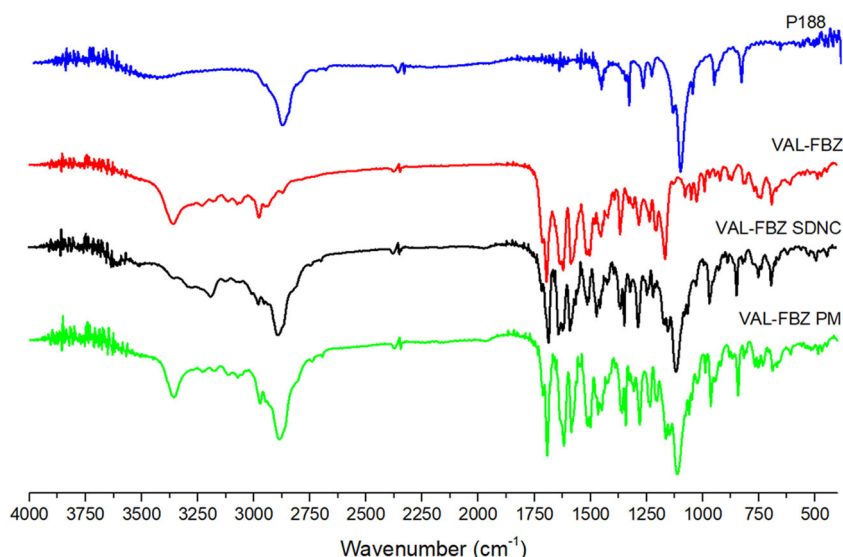**Fig. 13.** XRPD for pure VAL-FBZ and VAL-FBZ after its treatment with water

Fig. 14. FTIR of VAL-FBZ:P188 1:1 formulations and pure components

explained in terms of the Noyes-Whitney equation (23). Additionally, it has also been confirmed the beneficial effect in dissolution rate of simply dispersing these benzimidazole drugs in a poloxamer matrix (8) and the importance of achieving a homogeneous distribution, proved by Raman mapping imaging, which is crucial for ensuring a proper wetting and redispersion of hydrophobic nanoparticles. All of these mentioned aspects gathered in the SDNCs contribute to the improvement of the *in vitro* dissolution rate of the drugs. This last comparative parameter is proposed to be theoretically related to *in vivo* data, since the absorption of a drug is proportional to its concentration and the time it remains in a suitable absorptive region of the gastrointestinal tract (45) and both variables are included in the dissolution efficiency calculation. Therefore, the higher dissolution efficiency values achieved with the SDNCs result encouraging to

test the new formulations *in vivo*, since the enhance in bioavailability of benzimidazole drugs is strongly related to an increase in their efficacy (53,54).

CONCLUSIONS

Self-dispersible FBZ nanocrystals with markedly improved dissolution profiles were successfully obtained by a relatively simple process that included wet bead milling followed by a spray-drying step. Different stabilizers were tested and P188 was selected as the best excipient to assist during the drying process. Furthermore, results suggested the importance of the bead milling size in determining the suspension drug particle size which appears to be not influenced by either the stabilizer type or amount. The technology applied to FBZ was successfully transferred to produce self-dispersible VAL-FBZ nanocrystals, a new promising compound with *in vitro* anthelmintic activity, improving the *in vitro* dissolution performance of both drugs which suggests the potential of the process to be adapted to different compounds. The exhaustive characterization of the final products was critical in order to understand the systems and their behavior. It was possible to discard interactions between carrier and drug; however this characterization allowed to identify changes in the VAL-FBZ crystalline structure after the milling process that need to be study further in order to get a deeper understanding of the compound crystalline behavior.

Fig. 15. FTIR of VAL-FBZ:P188 1:1 formulations and pure components

Table 3. Solubility of FBZ and VAL-FBZ Physical Mixtures (PMs) and SDNCs Containing 50% of P188 (SDNC10 and SDNC11) in HCl 0.1 N at 37°C

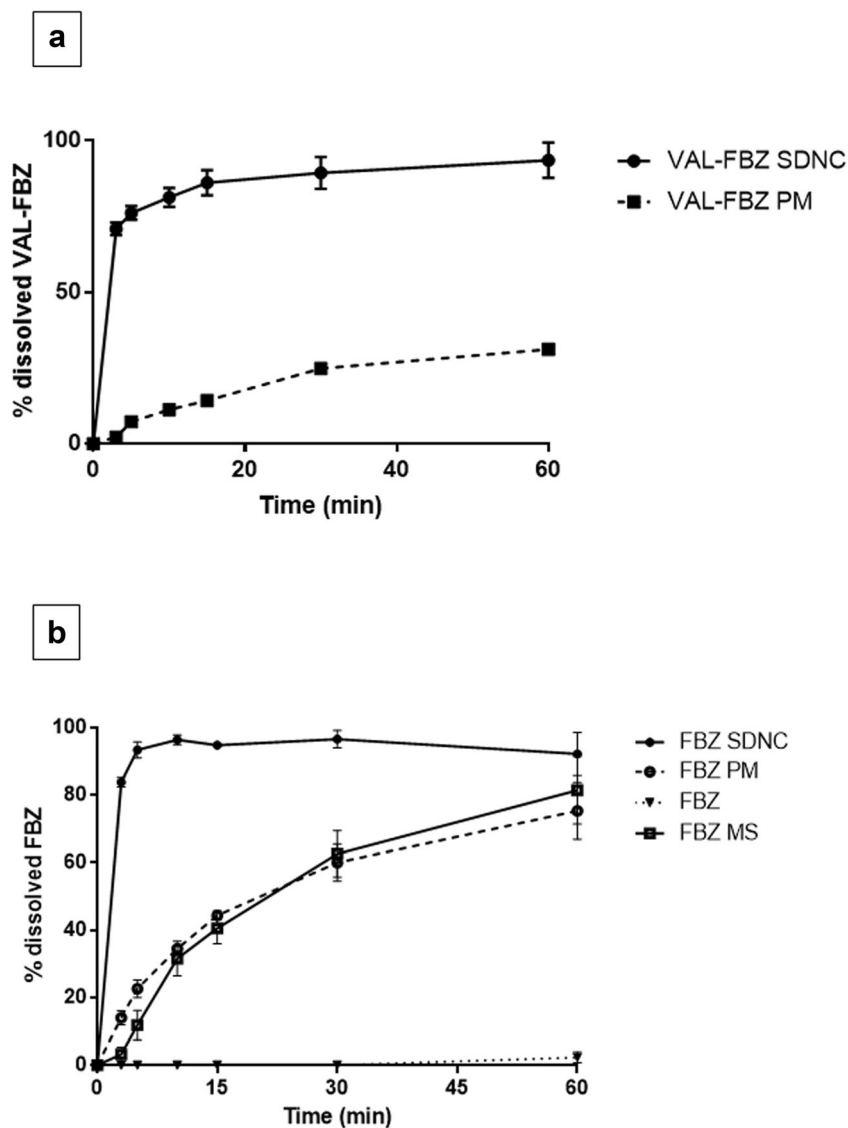|	Pure drug	PM	SDNCs
FBZ (mg.L^{-1})	36.5 ± 1.9	33.2 ± 2.5	45.3 ± 1.1
VAL-FBZ (mg.L^{-1})	173.5 ± 19.9	201.5 ± 27.1	325.9 ± 48.2
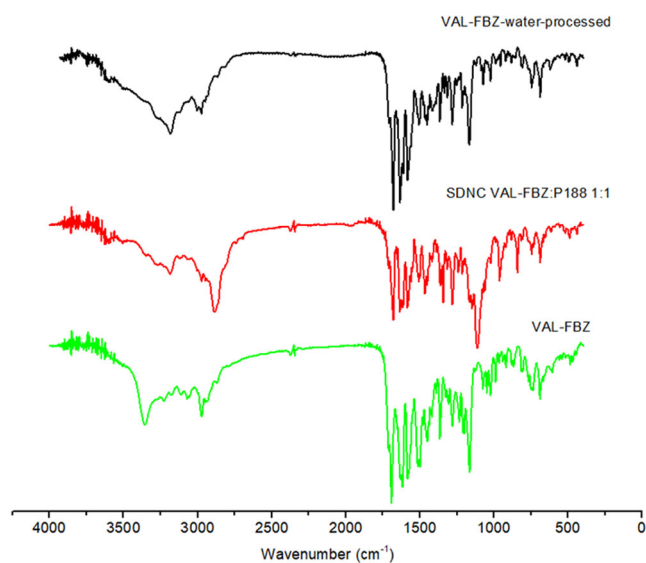
Fig. 16. **a** Dissolution profile of VAL-FBZ SDNC and PM. VAL-FBZ was not quantifiable during the assay of the pure drug. **b** Dissolution profile of FBZ and SDNC, the corresponding PM, the FBZ-marketed suspension, and pure FBZ

Table 4. Dissolution Efficiency (DE) of the FBZ and VAL-FBZ Formulations at Different Dissolution Times

	DE% 5 min	SD	DE% 30 min	SD	DE% 60 min	SD
FBZ	0.0	0.0	0.0	0.0	0.6	0.4
FBZ-marketed suspension	3.7	2.1	35.7	3.7	53.9	5.8
SDNC10 (FBZ)	60.6	1.1	89.7	1.4	92.1	2.9
PM FBZ	13.5	0.3	37.2	1.1	46.7	1.2
VAL-FBZ	0.0	0.0	0.0	0.0	0.0	0.0
SDNC11 (VAL-FBZ)	50.7	1.5	79.4	2.2	85.4	3.9
PM VAL-FBZ	2.6	0.8	13.9	0.9	21.0	1.0

ACKNOWLEDGMENTS

REFERENCES

1. Waller P. From discovery to development: current industry perspectives for the development of novel methods of helminth control in livestock. Vet Parasitol. 2006;139(1–3):1–14.
2. Torres-Acosta J, Mendoza-de-Gives P, Aguilar-Caballero A, Cuéllar-Ordaz J. Anthelmintic resistance in sheep farms: update of the situation in the American continent. Vet Parasitol. 2012;189(1):89–96.
3. Martin RJ, Wolstenholme AJ, Caffrey CR. Anthelmintics: from discovery to resistance II (san Diego, 2016). Int J Parasitol Drugs Drug Resist. 2016;6(3):297–8.
4. Kotze A, Prichard R. Anthelmintic resistance in Haemonchus contortus: history, mechanisms and diagnosis. Adv Parasitol. 2016;93: Elsevier:397–428.
5. Lambert SM, Nishi SM, Mendonça LR, da Silva Souza BMP, da Silva JF, da Silva GP, et al. Genotypic profile of benzimidazole resistance associated with SNP F167Y and F200Y beta-tubulin gene in Brazilian populations of Haemonchus contortus of goats. Vet Parasitol. 2017;8:28–34.
6. Nari A, Salles J, Gil A, Waller P, Hansen J. The prevalence of anthelmintic resistance in nematode parasites of sheep in southern Latin America: Uruguay. Vet Parasitol. 1996;62(3–4):213–22.
7. Mederos A, Carracelas B, Lara S, Pimentel S, Banchero G. Situación actual de la resistencia a las drogas antihelmínticas en ovinos en Uruguay. Rev INIA Urug. 2016;44:10–2.
8. Melian ME, Munguía AB, Faccio R, Palma S, Domínguez L. The impact of solid dispersion on formulation, using confocal micro Raman spectroscopy as tool to probe distribution of components. J Pharm Innov. 2018;13(1):58–68.
9. Munguía B, Michelena M, Melian E, Saldaña J, Ures X, Manta E, et al. Development of novel valerolactam-benzimidazole hybrids anthelmintic derivatives: diffusion and biotransformation studies in helminth parasites. Exp Parasitol. 2015;153:75–80.
10. Munguía B, Mendina P, Espinosa R, Lanz A, Saldaña J, Andina JM, et al. synthesis and anthelmintic evaluation of novel valerolactam-benzimidazole hybrids. Lett Drug Des Discov. 2013;10(10):1007–14.
11. Ku MS, Dulin W. A biopharmaceutical classification-based right-first-time formulation approach to reduce human pharmacokinetic variability and project cycle time from first-in-human to clinical proof-of-concept. Pharm Dev Technol. 2012;17(3):285–302.
12. Fenske DB, Cullis PR. Liposomal nanomedicines. Exp Opin Drug Deliv. 2008;5(1):25–44.
13. Letchford K, Burt H. A review of the formation and classification of amphiphilic block copolymer nanoparticulate structures: micelles, nanospheres, nanocapsules and polymersomes. Eur J Pharm Biopharm. 2007;65(3):259–69.
14. Schultheiss N, Newman A. Pharmaceutical cocrystals and their physicochemical properties. Crystal Growth Des. 2009;9(6):2950–67.
15. Stella VJ, He Q. Cyclodextrins. Toxicol Pathol. 2008;36(1):30–42.
16. Lee J, Choi J-Y, Park C. Characteristics of polymers enabling nano-comminution of water-insoluble drugs. Int J Pharm. 2008;355(1–2):328–36.
17. Van Drooge D, Hinrichs W, Visser M, Frijlink H. Characterization of the molecular distribution of drugs in glassy solid dispersions at the nano-meter scale, using differential scanning calorimetry and gravimetric water vapour sorption techniques. Int J Pharm. 2006;310(1–2):220–9.
18. Kohli K, Chopra S, Dhar D, Arora S, Khar RK. Self-emulsifying drug delivery systems: an approach to enhance oral bioavailability. Drug Discov Today. 2010;15(21–22):958–65.
19. Zhang T, Yang R, Yang S, Guan J, Zhang D, Ma Y, et al. Research progress of self-assembled nanogel and hybrid hydrogel systems based on pullulan derivatives. Drug Deliv. 2018;25(1):278–92.
20. Müller R, Keck C. Twenty years of drug nanocrystals: where are we, and where do we go? Eur J Pharm Biopharm. 2012;80(1):1–3.
21. Liu T, Yu X, Yin H, Möschwitzer JP. Advanced modification of drug nanocrystals by using novel fabrication and downstream approaches for tailor-made drug delivery. Drug Delivery. 2019;26(1):1092–103.
22. Liversidge GG, Cundy KC, Bishop JF, Czekai DA. Surface modified drug nanoparticles. Google Patents; 1992.
23. Keck CM, Müller RH. Drug nanocrystals of poorly soluble drugs produced by high pressure homogenisation. Eur J Pharm Biopharm. 2006;62(1):3–16.
24. Müller RH, Gohla S, Keck CM. State of the art of nanocrystals–special features, production, nanotoxicology aspects and intracellular delivery. Eur J Pharm Biopharm. 2011;78(1):1–9.
25. Paredes AJ, Llabot JM, Sánchez Bruni S, Allemandi D, Palma SD. Self-dispersible nanocrystals of albendazole produced by high pressure homogenization and spray-drying. Drug Dev Indust Pharm. 2016;42(10):1564–70.
26. Paredes AJ, Bruni SS, Allemandi D, Lanusse C, Palma SD. Albendazole nanocrystals with improved pharmacokinetic performance in mice. Ther Deliv. 2018;9(2):89–97.
27. Morales J, Watts A, McConville J. Formulating poorly water soluble drugs. In: Williams III RO, Watts AB, Miller DA, editors. 22. Springer; 2016. p. 165–213.
28. Choi J-Y, Yoo JY, Kwak H-S, Nam BU, Lee J. Role of polymeric stabilizers for drug nanocrystal dispersions. Curr Appl Phys. 2005;5(5):472–4.
29. Van Eerdenbrugh B, Van den Mooter G, Augustijns P. Top-down production of drug nanocrystals: nanosuspension stabilization, miniaturization and transformation into solid products. Int J Pharm. 2008;364(1):64–75.
30. Shegokar R, Müller RH. Nanocrystals: industrially feasible multifunctional formulation technology for poorly soluble actives. Int J Pharm. 2010;399(1–2):129–39.
31. Möschwitzer JP. Drug nanocrystals in the commercial pharmaceutical development process. Int J Pharm. 2013;453(1):142–56.
32. Yao J, Cui B, Zhao X, Wang Y, Zeng Z, Sun C, et al. Preparation, characterization, and evaluation of azoxystrobin nanosuspension produced by wet media milling. Appl Nanosci. 2018;8(3):297–307.
33. Ghosh I, Schenck D, Bose S, Ruegger C. Optimization of formulation and process parameters for the production of nanosuspension by wet media milling technique: effect of vitamin E TPGS and nanocrystal particle size on oral absorption. Eur J Pharm Sci. 2012;47(4):718–28.
34. Li M, Azad M, Davé R, Bilgili E. Nanomilling of drugs for bioavailability enhancement: a holistic formulation-process perspective. Pharmaceutics. 2016;8(2):17.
35. Cooper ER. Nanoparticles: a personal experience for formulating poorly water soluble drugs. J Control Release. 2010;141(3):300–2.

36. Junyaprasert VB, Morakul B. Nanocrystals for enhancement of oral bioavailability of poorly water-soluble drugs. Asian J Pharm Sci. 2015;10(1):13–23.

37. Yang H, Teng F, Wang P, Tian B, Lin X, Hu X, et al. Investigation of a nanosuspension stabilized by Soluplus® to improve bioavailability. Int J Pharm. 2014;477(1–2):88–95.

38. McKellar Q, Galbraith E, Baxter P. Oral absorption and bioavailability of fenbendazole in the dog and the effect of concurrent ingestion of food. J Vet Pharmacol Ther. 1993;16(2):189–98.

39. McKellar Q, Gokbulut C, Muzandu K, Benchaoui H. Fenbendazole pharmacokinetics, metabolism, and potentiation in horses. Drug Metab Dispos. 2002;30(11):1230–9.

40. Gokbulut C, Bilgili A, Hanedan B, McKellar Q. Comparative plasma disposition of fenbendazole, oxfendazole and albendazole in dogs. Vet Parasitol. 2007;148(3–4):279–87.

41. Mendina P, Munguía B, Espinosa R, Saldaña J, Domínguez L, Manta E. Inventorsderivados de la 2-amino-δ-valerolactama y benzimidazoles que presentan actividad antiparasitaria y en particular antihelmíntica de amplio espectro. Uruguay. 2014.

42. Paredes AJ, Camacho NM, Schofs L, Dib A, del Pilar ZM, Litterio N, et al. Ricobendazole nanocrystals obtained by media milling and spray drying: pharmacokinetic comparison with the micronized form of the drug. Int J Pharm. 2020;119501.

43. Camiletti BX, Camacho NM, Paredes AJ, Allemandi DA, Palma SD, Grosso NR. Self-dispersible nanocrystals of azoxystrobin and cyproconazole with increased efficacy against soilborne fungal pathogens isolated from peanut crops. Powder Technol. 2020.

44. Karavas E, Georgarakis M, Docoslis A, Bikiaris D. Combining SEM, TEM, and micro-Raman techniques to differentiate between the amorphous molecular level dispersions and nanodispersions of a poorly water-soluble drug within a polymer matrix. Int J Pharm. 2007;340(1–2):76–83.

45. Khan K. The concept of dissolution efficiency. J Pharm Pharmacol. 1975;27(1):48–9.

46. Paredes AJ, Litterio N, Dib A, Allemandi DA, Lanusse C, Bruni SS, et al. A nanocrystal-based formulation improves the pharmacokinetic performance and therapeutic response of albendazole in dogs. J Pharm Pharmacol. 2018;70(1):51–8.

47. Freitas C, Müller RH. Spray-drying of solid lipid nanoparticles (SLNTM). Eur J Pharm Biopharm. 1998;46(2):145–51.

48. Wang Y, Zheng Y, Zhang L, Wang Q, Zhang D. Stability of nanosuspensions in drug delivery. J Control Release. 2013;172(3):1126–41.

49. Sharma OP, Patel V, Mehta T. Design of experiment approach in development of febuxostat nanocrystal: application of Soluplus® as stabilizer. Powder Technol. 2016;302:396–405.

50. Nibbering ET, Dreyer J, Kühn O, Bredenbeck J, Hamm P, Elsaesser T. Vibrational dynamics of hydrogen bonds. Analysis and control of ultrafast photoinduced reactions. Springer; 2007. p. 619–87.

51. Lanusse CE, Prichard RK. Clinical Pharmacokinetics and Metabolism of Benzimidazole Anthelmintics in Ruminants. Drug Metab Rev. 1993;25(3):235–79.

52. McKellar Q, Scott E. The benzimidazole anthelmintic agents-a review. J Vet Pharmacol Ther. 1990;13(3):223–47.

53. Pensel P, Paredes A, Albani CM, Allemandi D, Bruni SS, Palma SD, et al. Albendazole nanocrystals in experimental alveolar echinococcosis: enhanced chemoprophylactic and clinical efficacy in infected mice. Vet Parasitol. 2018;251:78–84.

54. Pensel PE, Gamboa GU, Fabbri J, Ceballos L, Bruni SS, Alvarez LI, et al. Cystic echinococcosis therapy: Albendazole-loaded lipid nanocapsules enhance the oral bioavailability and efficacy in experimentally infected mice. Acta Trop. 2015;152:185–94.